Adult visual deprivation engages associative,

presynaptic plasticity of thalamic input to cortex

Sachiko Murase[1], Daniel Severin[2,3], Louis Dye[4], Lukas Mesik[2,3], Cristian Moreno[2,3], Alfredo Kirkwood[2,3] and Elizabeth M. Quinlan[5]

[1]Department of Biology, University of Maryland, College Park, MD 20742,

[2]Mind/Brain Institute, Johns Hopkins University, Baltimore MD 21218,

[3]Department of Neuroscience, John Hopkins University, Baltimore, MD 21205,

[4]NICHD Eunice Kennedy Shriver, Microscopy & Imaging Core, NIH, Bethesda, MD 20892,

[5]Department of Neuroscience, University of Wisconsin, Madison, Madison WI 53507

Abstract

Associative plasticity at thalamocortical synapses is thought to be constrained by age in the mammalian cortex. However, here we show for the first time that prolonged visual deprivation induces robust and reversible plasticity at synapses between first order visual thalamus and cortical layer 4 pyramidal neurons. The plasticity is associative and expressed by changes in presynaptic function, thereby amplifying and relaying the change in efferent drive to the visual cortex.

Introduction (3169 main text)

Robust receptive field plasticity can be rejuvenated in the adult rodent visual cortex by visual deprivation through prolonged dark exposure (DE) and subsequent light reintroduction (LRx) (He et al., 2006, 2007). In amblyopic rats, visual stimulation following dark exposure strengthen thalamic input to cortical neurons, and drives the full recovery of visual acuity through the amblyopic eye (He et al., 2007; Montey and Quinlan, 2011; Eaton et al., 2016). The rejuvenation of plasticity by DE has been also demonstrated in felines (Duffy et al., 2016) and mice (Stodieck et al., 2014; Jeon et al., 2022). However, our understanding of how prolonged DE promotes the recovery from amblyopia is incomplete.

Visual deprivation induces a well-documented homeostatic increase in the amplitude of postsynaptic AMPAR-dependent excitatory postsynaptic currents at cortico-cortical synapses in the primary visual cortex (Wen and Turrigiano, 2024). In adult rodents, DE increases the amplitude of mEPSCs in L2/3 neurons in V1 (Goel et al., 2006; Goel and Lee, 2007), and requires the immediate early gene Arc (Gao et al., 2010). The regulation of mEPSC amplitudes by DE is observed at intra-layer synapses between L2/3 neurons but not at thalamic inputs to cortical neurons (Petrus et al., 2014, 2015; Chokshi et al., 2019). Prolonged DE increases the expression of the GluN2b subunit of the NMDAR in adult rodent V1 (He et al., 2006), which endows NMDARs with high agonist affinity, high open probability and slow deactivation kinetics. High GluN2b levels are associated with a low induction threshold for correlation-based plasticity (Cooper

and Bear, 2012; Lee and Kirkwood, 2019). Accordingly, the DE-induced increase in GluN2b subunit content at excitatory synapses on layer 2/3 pyramidal neurons lowers the threshold for Hebbian synaptic strengthening. The DE-induced increase in EPSC amplitude is the result of subsequent synaptic potentiation and is blocked by a GluN2b antagonist (Bridi et al., 2018). Interestingly, magnetic resonance spectroscopy reveals that brief DE (60 min) increases the local concentration of glutamine/glutamate in human adult V1, demonstrating the universality in the homeostatic response to visual deprivation (Min et al., 2023).

In contrast, associative plasticity mediated by potentiation/depression of postsynaptic EPSC amplitudes is constrained over development particularly at thalamo-cortical (TC) synapses. In the barrel cortex, pairing-induced LTP, NMDAR-dependent LTD and silent synapses are all lost with age (Crair and Malenka, 1995; Isaac et al., 1997; Feldman et al., 1998). Similarly, in the primary visual cortex, LTP in layer 4 induced by stimulation of white matter is also lost early in development, at a time when associative plasticity is robust at L4-L2/3 synapses (Jiang et al., 2007). In cat V1, the loss of mesoscopic anatomical plasticity of geniculocortical afferents induced by monocular deprivation (MD) during the critical period (Antonini and Stryker, 1993) proceeds the loss of synaptic plasticity at cortico-cortical synapses (Wiesel and Hubel, 1963; Antonini and Stryker, 1996).

However, recent work demonstrates the response properties of neurons in the dorsal lateral geniculate nucleus (dLGN) can be modified well into adult life. Monocular

deprivation in adults induces a shift in ocular preference of dLGN neurons (Qin et al., 2023) and dLGN axonal boutons in layer 1 of primary visual cortex (Jaepel et al., 2017).

Thalamic neurons respond to perceptual learning in human adults (Yu et al., 2016). Calcium imaging of dLGN boutons reveals changes in stimulus selectivity following MD in both juveniles and adult mice (Huh et al., 2020). Whisker trimming in adult mice can reduce thalamic axon length of thalamic axons and synapse number (Oberlaender et al., 2012).

Extraordinary manipulations can also re-engage plasticity at adult TC synapses. In barrel cortex, peripheral nerve transection strengthens spared TC synapses (Yu et al., 2012; Chung et al., 2017). TC synapses are a locus for the expression of cross-modal plasticity, and vice versa (Petrus et al., 2014; Chung et al., 2017). Environmental enrichment, which promotes plasticity in adults (Sale et al., 2007) regulates plasticity in TC synapses through a presynaptic mechanism (Mainardi et al., 2010).

Our previous work has identified thalamocortical synapses as an important locus for the rejuvenation of plasticity by DE/LRx (Murase et al., 2017). Here we use a set of orthogonal approaches to ask if DE/LRx enhances plasticity at adult TC synapses. We find that prolonged DE induces a decrease in neurotransmitter release probability at TC synapses, and corresponding changes in presynaptic vesicle geometry, molecular organization and visually-evoked calcium influx of thalamic axonal boutons. The response of TC synapse is reversible and associative, thereby amplifying and relaying the change in efferent drive to the visual cortex.

Results

To ask if prolonged DE regulated the efficacy of feed-forward synapses from first order thalamus to L4 in adult mouse visual cortex, we used optogenetically isolated the activity of dLGN axons in acute slices (Fig. 1a). AAV5-CaMKIIa-hChR2(H134R)-mCherry was delivered to dLGN in adult C57BL/6J mouse 3 weeks prior to recording (>postnatal day 90, P>90). The quantal amplitude of optogenetically evoked EPSCs at the stimulation intensity evoking 50% response (470 nm, 3 msec), recorded in V1b L4 neurons, was estimated following desynchronization by substituting Sr^{2+} for Ca^{2+} (Fig. 1b, c (Dodge Jr. et al., 1969)). Monosynaptic evoked EPSCs (evEPSCs) in V1b Layer 4 neurons, desynchronized in the presence of TTX and 4-AP (Fig. 1b, c (Petreanu et al., 2009; Whitt et al., 2022)) in control normal adult mice (NR, raised in a normal 12/12 cycle) had a mean amplitude of 13 pA, as expected, which was unchanged following 10 days of DE. Brief LRx (2 h) induced a small, but significant decrease in evEPSC amplitude (mean±sem: NR = 12.9±0.7 pA, DE = 13.0±0.6 pA, LRx = 11.2±0.4 pA; n = 31, 26, 25 cells from 6, 5, 5 subjects, respectively, Kruskal-Wallis H (2) = 10.39, p = 0.0055, *post hoc* Dunn's multiple comparison test, *p<0.05; Fig. 1c,d).

In contrast, DE/LRx induced robust changes in presynaptic function at TC synapses. Optogenetically-evoked EPSCs were recorded in L4 neurons in response to repetitive, 15 spikes at 25 Hz). Raw (Fig. 1e) and normalized TC EPSC amplitudes reveal significant short-term depression of TC transmission in response to repetitive stimulation, as expected. The response to repetitive stimulation is modified by DE and LRx (Two-way ANOVA; for interaction F (28, 1095) = 0.5042, p=0.9857; for visual

experience F (2, 1095) = 71.36, *p<0.0001, *post hoc* Bonferroni *p<0.05, n = 32, 23, 21 cells from 8, 6, 5 subjects, respectively; Fig. 1f). Normalized steady state EPSCs wer increased by DE and decreased by LRx, (NR = 0.31±0.31, DE = 0.38±0.05, LRx = 0.19±0.02; n = 32, 23, 21 cells from 8, 6, 5 subjects respectively; Kruskal-Wallis H (2) = 11.22, *p = 0.0037, *post hoc* Dunn's multiple comparison test; *p<0.05; Fig. 1g). The paired pulse ratio (PPR) calculated from the response to the second relative to the first stimulus increased following DE and decreased following LRx (NR = 0.41±0.05, DE = 0.56±0.04, LRx = 0.31±0.04; n = 32, 23, 21 cells from 8, 6, 5 subjects respectively; Kruskal-Wallis H (2) = 13.97, *p = 0.0009, *post hoc* Dunn's multiple comparison test, *p<0.05; Fig. 1h). Accordingly, the presynaptic vesicle release probability derived from paired pulse ratio, calculated as in Bridi et al. (Bridi et al., 2020) based on Wesseling and Lo (Wesseling and Lo, 2002). (NR = 0.50±0.03, DE = 0.39±0.02, LRx = 0.51±0.03; n = 32, 23, 21 cells from 8, 6, 5 subjects respectively; One-way ANOVA, F = 4.699, *p = 0.012, post hoc Tukey, *p<0.05; Fig. 1i). The estimated vesicle recovery rate is unchanged following DE and decreased by LRx (NR = 4.0±0.67, DE = 3.6±0.44, LRx = 2.4±0.22; n = 32, 23, 21 cells from 8, 6, 5 subjects respectively, Kruskal-Wallis H (2) = 6.838, *p = 0.0327, *post hoc* Dunn's multiple comparison test, *p<0.05; Fig. 1j). Thus, prolonged visual deprivation and light reintroduction engage plasticity of presynaptic function at adult TC synapses.

Presynaptic function is defined by molecular and structural parameters. We therefore quantified fundamental features of synaptic ultrastructure in transmission electron micrographs. Presynaptic area has been shown to be a good predictor of presynaptic

origin (Nahmani and Erisir, 2005). Accordingly, we observed a bimodal distribution of presynaptic area (Fig. 2a). Synapses in the top 15th percentile of presynaptic area (>0.6 μm^2) had larger cleft width and PSD length, as expected for TC synapses (cleft width: 21.6±0.3 nm vs. 19.8±0.1 nm, $p=2.2e^{-7}$; PSD length: 472±30 nm vs. 350±8 nm *$p<1.3e^{-7}$, Student's T-test , n=230, 34). Larger, presumptive TC synapses also had more synaptic vesicles in contact with the presynaptic membrane opposing the PSD ("docked" synaptic vesicles; TC = 4.63±0.37, CC = 3.11±0.12; $p=6.9e^{-6}$, Student's T-test) and a larger area was occupied by synaptic vesicles (synaptic vesicle zone, SVZ, TC = 0.16±0.01 μm^2, CC = 0.26±0.2 μm^2; *$p=5.9e^{-8}$, Student's T-test*).*

We performed a bivariate analysis on the impact of DE and LRx on each of these ultrastructural variables versus presynaptic area. Prolonged DE induced widespread changes in ultrastructure, including a significant decrease in cleft width, prominent in smaller synapses (Con = 20.0±0.1 nm, DE = 19.0±0.2 nm; Mann-Whitney Test, *p<0.001) and a decrease in PSD length, prominent in larger synapses (Con = 366±17 nm, DE = 335±12 nm; Mann-Whitney Test, *p=0.02). Docked vesicle numbers were increased in smaller synapses and decreased in larger synapses (Con =3.14±0.11, DE = 3.91±0.11; Mann-Whitney Test, *p<0.001). DE increased the total area occupied by synaptic vesicles (Synaptic vesicle area, SVZ area (Con = 0.17±0.9 μm^2, DE = 0.25±0.3 μm^2; Mann-Whitney Test, p<0.001, n = 264 and 219 synapses respectively) in both larger and smaller synapses.

In contrast, LRx induced relatively few changes in synaptic ultrastructure. We observed no change in cleft width or PSD length following LRx (cleft: DE = 19.0±0.2 nm, LRx = 19.2±0.1 nm; Mann-Whitney Test, p=0.34; PSD: DE = 335±12 nm, LRx = 328±7 nm; Mann-Whitney Test, p=0.23). However following LRx, the number of docked vesicles was decreased at smaller synapses and increased at larger synapses (DE = 3.91±0.11, LRx = 3.72±0.12; Mann-Whitney Test, *p=0.04, Fig. 2b). Brief LRx reversed DE-induced change in SVZ area (DE = 0.25±0.3 μm^2, LRx = 0.19±0.1 μm^2, Mann-Whitney Test, *p<0.001, n = 219 and 320 synapses, respectively). Thus, DE induces widespread changes in presynaptic ultrastructure, only a subset of which are reversed by a brief LRx.

The declustering/clustering of synaptic vesicles was reminiscent of declustering/clustering of components of the presynaptic cytomatrix following action potential suppression reported in cultured hippocampal neurons (Glebov et al., 2016, 2017). To ask if DE/LRx impacted presynaptic molecular organization, we adapted a FRET-based intramolecular proximity assay to quantify *in situ* clustering of the cytomatrix protein bassoon (Bsn) in axons synapsing on layer 4 of adult mouse V1b (360±40 μm from dura) following DE/LRx.

We utilized a validated monoclonal primary antibody and a pair of anti-mouse secondary antibodies conjugated to either a FRET acceptor or a FRET donor (1:1; Fig. 3a). Forster resonance transfer (FRET) distance is limited to ~10 nm, therefore a change in $FRET_{Acceptor/Donor}$ reports a change in intramolecular distance of the secondary

antibodies. We confirmed the proximity assay is sensitive to intramolecular distance, as $FRET_{A/D}$ decreased with serial dilution of the secondary antibody mix (500x, 1.24±0.004; 2000x, 0.95±0.003; 8000x, 0.78±0.01, n = 2343, 2304, 970 puncta, respectively. One-way ANOVA, F = 1731, p = 0.0001, *post hoc* Tukey, *p<0.05, Fig. 3b). To identify thalamic axons, we quantified $FRET_{A/D}$ that colocalized with a marker for thalamic axons (vesicular transporter 2;VGluT2 (Nahmani and Erisir, 2005; Coleman et al., 2010)). DE decreased $FRET_{A/D}$, indicative of an increase in intra-molecular Bsn distance, and LRx increased $FRET_{A/D}$, indicative of a decrease in intramolecular Bsn distance (Con =1.22±0.07, DE = 0.88±0.02, LRx = 1.28±0.03; n = 6, 4, 4 subjects, respectively, One-way ANOVA, F = 14.3, p < 0.001, *post hoc* Tukey, *p<0.05; Fig. 3c,d). Neither DE nor LRx changed the total level of Bsn when visualized with a single secondary antibody (Con = 45.9±0.9; DE = 44.2±1.4; LRx = 47.4±1.7; n = 6, 5, 6 subjects, respectively; One-way ANOVA, F = 1.0, p = 0.41; Fig. 3e). Thus, DE and LRx impact the molecular geometry of presynaptic active zones of thalamic axons.

Clustering/unclustering of Bsn has been correlated with changes in the abundance of active zone VGCCs (Glebov et al., 2017), a key determinant of presynaptic release probability. As an additional test of the hypothesis that DE/LRx modifies presynaptic function of TC synapses in adult V1, we quantified the magnitude of visually-evoked calcium transients at thalamic boutons in layer 4 in awake head-fixed mice (Fig. 4a). AAV5-Ef1a-DIO-Synaptophysin-GCaMP6s was delivered to dLGN in adult VGluT2-Cre mice 3 weeks prior to recording. Thalamic axons were imaged in V1b (average cortical depth: 320 μm). Calcium transients in axonal boutons were evoked by drifting square

wave gratings delivered to contralateral or ipsilateral the eye. Visually-responsive boutons were included for analysis if 1) peak ΔF/F value 0.25 - 2.0 sec after visual stimulation onset at any direction for $\geq$ 40% trials exceeded 4 x STD of baseline (F_0, -1.0 to 0 sec), and 2) mean ΔF/F during the rising phase of response (0.25 to 1.0 sec after visual stimulus onset) exceeded 2 x signal/noise ratio. We observed the expected tuning of individual boutons for visual stimulus orientation (0.05 cpd ,100% contrast). ΔF/F of calcium transients evoked in dLGN boutons by high contrast drifting grating in the preferred orientation was decreased by DE and recovered by LRx (Con =1.065±0.03, DE = 0.48±0.03, LRx = 0.94±0.0; n = 4, 4, 4 subjects, respectively; One-way ANOVA, F = 9.9, p = 0.005, *post hoc* Tukey, *p<0.05; Fig. 4b-d). Thus, DE/LRx in adulthood engages robust associative presynaptic plasticity at TC synapses.

Discussion

Investigations of synaptic plasticity engaged by visual deprivation in the adult mammalian cortex have focused on cortical inputs to superficial neurons, as associative plasticity at thalamic inputs had been shown to be constrained by age. Here we show for the first time that prolonged visual deprivation induces robust and reversible plasticity at thalamocortical synapses in adult mice. The plasticity is associative, and expressed by changes in presynaptic function.

This finding was unexpected but supported by evidence from 4 complementary experimental techniques. 1) Optogenetic control of thalamic axons revealed that presynaptic release probability was reversibly decreased by prolonged DE. 2) synaptic ultrastructure revealed that DE reversibly declustered synaptic vesicles and decreased the number of docked vesicles at TC synapses. 3) A FRET-based intramolecular proximity analysis revealed reversible declustering of the presynaptic scaffold Bsn in thalamic axon boutons (Nahmani and Erisir, 2005; Coleman et al., 2010). 4) Intravital calcium imaging revealed that DE reversibly reduced visually evoked calcium transients in dLGN boutons in cortical layer 4 (Sun et al., 2016).

We were surprised that the well-documented homeostatic increase in EPSC amplitudes in supragranular cortical layers following DE is not expressed at TC synapses. Indeed, optogenetically-evoked TC EPSC amplitudes in layer 4 neurons are unchanged by prolonged DE in adults, as previously described in juveniles (Petrus et al., 2014). The absence of strong postsynaptic response to manipulations of visual experience may explain the paucity of examples of TC plasticity in adults.

The response to prolonged visual deprivation is one of many ways in which TC synapses are differentiated from CC synapses. Our ultrastructural analysis of excitatory synapses in V1 layer 4 revealed opposing changes at small presumptive CC and large presumptive TC synapses, corroborating our finding that these two classes of synapses respond differently to prolonged visual deprivation. Differences in presynaptic area, molecular composition, neurotransmitter release probability may contribute to the developmental constraint on associative plasticity at TC synapses (Stratford et al., 1996; Ziv et al., 1999; Chung et al., 2002; Yanagisawa et al., 2004; Kloc and Maffei, 2014). Differential sensitivity to neuromodulators and neurotrophins also distinguishes plasticity in cortical layer 4 and superficial layers (Crozier et al., 2007; Frantz et al., 2020).

Recent work in hippocampal slice culture demonstrates that prolonged actional potential suppression can engage a heterogeneous synaptic response mediated by changes in pre- and post- synaptic function, resulting in a reduction in excitatory synaptic density and an increase in the strength of retained synapses (Wise et al., 2024). Similarly, TTX induces a decrease in the functional connectivity between pairs of excitatory neurons but an increase in the strength and Pr of synapses that retained connectivity (Mitra et al., 2012). However, we did not observe a similar heterogeneity in response to prolonged dark exposure in adult mouse V1, and found no evidence for homeostatic changes in presynaptic function as have been described in cultured mammalian neurons and fly neuromuscular junction (Bacci et al., 2001; Murthy et al., 2001; Burrone

et al., 2002; Echegoyen et al., 2007; Tokuoka and Goda, 2008; Davis and Müller, 2015; Harris and Littleton, 2015; Delvendahl and Müller, 2019; Valakh et al., 2023).

It is interesting to speculate that prolonged deprivation is required to engage presynaptic plasticity at TC synapses. Presynaptic plasticity may compensate for the developmental loss of postsynaptic plasticity. Indeed, brief (3 days) MD does not change presynaptic release probability in optogenetically evoked TC EPSCs during the postnatal critical period (Linden et al., 2009; Wang et al., 2013).
Presynaptic depression, mediated by depletion of neurotransmitter vesicles or activation of Gi/o via a retrograde messenger, is widespread in the nervous system. Notably, inhibition of adenosine production or A_1-adenosine receptor signaling in the auditory thalamus can reactivate plasticity (Blundon et al., 2017) and adenosine release from astrocytes has been implicated in the timing of the CP (Andrade-Talavera et al., 2023). Thus, one intriguing possibility is that a presynaptic receptor coupled to Gi/o is engaged by a retrograde messenger released by cortical neurons (Lu and Mackie, 2021) following prolonged DE .

We found the expected bimodal distribution of presynaptic terminal area of excitatory synaptic profiles in V1 layer 4, (Nahmani and Erisir, 2005; Coleman et al., 2010)) which aligns with estimates of the number of thalamic inputs onto L4 neurons and corroborates previous findings that presynaptic size is a good predictor of presynaptic origin (Schoonover et al., 2014; Bopp et al., 2017). However, we cannot rule out the possibility that the largest 15% of excitatory synapses identified by TEM in V1 layer 4

represent a mix of TC and CC synapses, and that initial bouton size/strength is an important determinant of sensitivity to DE/LRx. Recent work demonstrates that a size distinction between TC and CC synapses is not present in supragranular layers of mouse V1 (Balcioglu et al., 2023).

Synaptic vesicles that closely oppose the active zone were used as a proxy for docked vesicles, as transmission electron microscopy does not have sufficient resolution to identify primed or tethered vesicles. Flash and freeze analysis of dentate gyrus granular cells reveals overlap between that the docked vesicle pool and readily releasable pool (Borges-Merjane et al., 2020) which supports the positive correlation between docked vesicle number and presynaptic release probability (Kaeser and Regehr, 2017).

Our work confirms that cleft widths at CNS synapses are maintained within a narrow range (Zuber et al., 2005), which may stabilize transsynaptic nanocolumns and limit neurotransmitter diffusion (Zheng et al., 2017)(Cole and Reese, 2023). However, prolonged DE induced a decrease in cleft width at smaller presumptive CC synapses, demonstrating maintenance at sub-optimal values (Savtchenko and Rusakov, 2007).

DE also decreased the size of PSD in larger, presumptive TC synapses. However, these changes occurred in the absence of a corresponding change in the amplitudes of Sr^{2+}-evEPSCs. Although PSD size has been shown to covary with spine volume, the number of AMPARs, AMPAR nanodomains, and EPSC amplitudes (Nair et al., 2013; Meyer et al., 2014; Borczyk et al., 2019; Hosokawa et al., 2021), our results suggest

that PSD size can be independent of AMPAR density, and is consistent with the observation that the PSD extends beyond nanodomains (Masch et al., 2018).

We used a intramolecular proximity assay, applied to cortical circuits *in situ* for the first time, to demonstrate that DE and LRx reversibly organized the molecular geometry of the presynaptic cytomatrix protein Bsn (Gundelfinger et al., 2016). Bsn clustering/declustering induced parallel, reversible changes in vesicle pool geometry by DE and LRx. We found that in TC synapses of the adult V1, prolonged DE induced a declustering of Bsn that was correlated with a reduction in visually-evoked calcium magnitudes and neurotransmitter release probability. Similarly, in culture hippocampal neurons, bassoon deletion reduced SV release competency measured by genetically encoded synaptic transmission reporter synapto-pHluorin (Davydova et al., 2014). In contrast, in cultured hippocampal neurons, AP suppression induced reversible Bsn declustering, increased density of Cav2.1 at presynaptic active zones and increased amplitudes of AP-evoked calcium transients (Glebov et al., 2017).

Deletion of Bsn decreases vesicle release "competence" and dysregulation of PKA phosphorylation of synapsin (Montenegro-Venegas et al., 2022). Ours is the first investigation of Bsn clustering on presynaptic function at boutons that do not express the vesicle organizing protein synapsin (Favre et al., 1986; Finger et al., 1990; Haas et al., 1990; Mandell et al., 1992; Owe et al., 2013).

Our findings suggest that synaptic plasticity can be regulated by experience at even the most recalcitrant synapses. Presynaptic depression may serve to lower the threshold for subsequent synaptic plasticity at thalamocortical synapses, allowing reorganization or recovery of receptive fields following loss in efferent drive (Lee and Kirkwood, 2019).

Materials and methods (1897)

Subjects

C57BL/6J mice were purchased from Jackson Laboratory (Bar Harbor, ME, USA). Equal numbers of adult (>P90, up to P170) males and females were used. Mice were raised in a 12 h light/dark cycle. All procedures conformed to the guidelines of the University of Maryland Institutional Animal Care and Use Committee. Experiments were performed (or subjects were sacrificed) 6 h into the light phase of a 12:12 h light/dark cycle.

Electron Micrograph

Mice were transcardially perfused fixed with 2.5% glutaraldehyde, 4% paraformaldehyde (PFA) in phosphate buffered saline (PBS, pH 7.4). Brains were post-fixed overnight, then kept in 0.01% NaN_3 in PBS at 4°C. Coronal sections (100 microns) were made using Leica vibratome (VT1000), and V1b and hippocampal commissure were isolated. All sections were rinsed in 0.1M sodium cacodylate buffer. The following processing steps were then carried out using the variable wattage Pelco BioWave Pro microwave oven (Ted Pella, Inc., Redding, CA): post-fixed in 1% osmium tetroxide made in 0.1 M sodium cacodylate buffer, rinsed in double distilled water (DDW), 2% (aq.) uranyl acetate enhancement, DDW rinse, ethanol dehydration series up to 100% ethanol and propylene oxide, followed by a Embed-812 resin (Electron Microscopy Sciences, Hatfield, PA) infiltration series up to 100% resin. The epoxy resin was polymerized for 20 h in an oven at 60°C. Ultra-thin sections were cut on a Leica EM-UC7 Ultramicrotome (90 nm). Thin sections were picked up and placed on 200 mesh

cooper grids and post-stained with uranyl acetate and lead citrate. Imaging was accomplished using a JEOL-1400 Transmission Electron Microscope operating at 80kV and an AMT BioSprint-29 camera.

FRET-based molecular proximity assay

Subjects were anesthetized with 4% isoflurane in O_2 and perfused with PBS followed by 4% PFA in PBS. The brains were post-fixed in 4% PFA for 24 h, followed by 30% sucrose for 24 h, and cryo-protectant solution for 24 h (0.58 M sucrose, 30% (v/v) ethylene glycol, 3 mM sodium azide, 0.64 M sodium phosphate, pH 7.4). Coronal sections (40 µm) were cut on a Leica vibratome (VT1000). Sections were blocked with 4% normal goat serum (NGS) containing 0.4% TritonX-100 and 0.1% Tween-20 in PBS for 30 min. The primary antibody was presented in a blocking solution overnight at 4°C, followed by the secondary antibody for 6 h.

Following antibodies/dilutions were used: Monoclonal mouse anti-Bsn (NeuroMab) RRID: AB_2895685, 1:1000, goat anti-mouse IgG Alexa-568 conjugated (Thermo Fisher Scientific) RRDI: AB_2534072, 1:1000, goat anti-mouse IgG Alexa-647 conjugated (Thermo Fisher Scientific) RRID: AB_2535804, 1:1000, unless the dilution is specified. FRET experiments were performed with an anti-Bsn monoclonal mouse antibody and a 50:50 mixture of the secondary antibody conjugated to fluorescent donor and fluorescent acceptor.

Images were acquired on a Leica SP5x confocal microscope with a 60X Oil lens (HCX PL APO CS, NA = 1.4) at Ex = 543 nm, with bandpass filters for Alexa568: 560 – 615 nm, Alexa-647: 650 – 720 nm. Bsn puncta were analyzed using a single Z-section

image after the threshold function (auto threshold + 20) was applied, and were then identified by size exclusion (0.2–2.0 μm^2) using the “analyze particles” function in Fiji (NIH).

Preparation of slices and optogenetic isolation of thalamocortical synapse

Isolation of thalamic inputs to V1 was achieved by optogenetic approach: injection of AAV5-CaMKIIa-hChR$_2$(H134R)-mCherry (addgene, Cat# 26975-AAV5, 1.4 x 10^{13} GS/mL, 300 μl) to adult C57BL/6J mouse dLGN (from Bregma AP: 2.3 mm, ML: 2.0 mm, DV: 2.4 mm) 3 weeks prior to recording at >postnatal day 90 (P>90). Each mouse was anesthetized using isoflurane vapors and, after disappearance of the corneal reflex, transcardially perfused with ice-cold dissection buffer containing (in mM): 212.7 sucrose, 5 KCl, 1.25 NaH_2PO_4, 10 $MgCl_2$, 0.5 $CaCl_2$, 26 $NaHCO_3$, and 10 dextrose, bubbled with 95% O_2/5% CO_2 (pH 7.4). The brain was rapidly removed, immersed in ice-cold dissection buffer and sectioned (300 μm) using a vibratome (Leica VT1200S). Visual cortical slices were transferred to artificial cerebrospinal fluid (ACSF), incubated at 30 °C for 30 min, and then kept at room temperature for 30 min until they were transferred to the recording chamber. ACSF was similar to dissection buffer except that sucrose was replaced by 124 mM NaCl, $MgCl_2$ was lowered to 1 mM, and $CaCl_2$ was raised to 2 mM. Visualized whole-cell recordings were made from principal neurons in layer 4 of V1 with glass pipettes (3-5 MΩ) filled with (in mM) 8 KCl, 125 cesium gluconate, 10 HEPES, 1 EGTA, 4 MgATP, 0.5 NaGTP, and 5 QX-314 (pH 7.2 to 7.3 and 280 to 295 mOsm). Biocytin (1 mg/ml) was added to the internal solution for post hoc cell identification. EPSCs were recorded in voltage–clamp at −70 mV in the

presence of 100 μM APV and 20 μM bicuculine. ChR2-containing axon terminals were activated using a 470 nm wavelength LED (3 ms duration; Thorlabs) through a 40x objective lens. To quantify the response to repetitive optogenetic stimulation, 15 light pulses were delivered at 25 Hz. The minimal light intensity that evoked 100% responses for all the pulses was used (range from 77.8 to 4799.8 mW, given the variability in ChR2 expression after the virus transfection). The shape of the EPSCs was examined, and cells were excluded from analysis if the rising phase exhibited any inflection points, which could indicate a polysynaptic response. The paired pulse ratio was calculated as 2nd EPSC/1st EPSC. The normalized EPSC at steady state was calculated as the mean of 11th to 15th EPSCs. The release probability and the recovery rate were calculated as described in Bridi et al., 2020 based on Wesseling and Lo, 2002. Briefly, equations (2) and (3) were derived from equation (1) as shown below:

$$\frac{dn}{dt} = \alpha \cdot (\mathrm{N} - n) - \beta \cdot n \tag{1}$$

"Where α denotes the recovery rate, β denotes the release probability, n represents the vesicles available for release, and N represents the total number of vesicles in the ready releasable pool.

$$fe = \frac{r(1)}{r(\infty)} \cdot \left(1 - e\frac{-\alpha}{v}\right) \tag{2}$$

$$fe = \frac{r(1)}{\sum_{i=1}^{S} r(i) \cdot e^{\frac{-\alpha \cdot (S-i)}{v}}} \tag{3}$$

Where fe is the initial release probability, $r(1)$ is the amount of transmitter released by the first stimulus in the train, $r(\infty)$ represents the release at steady-state during the train, v is the stimulation frequency, S is the total number of stimuli in the train, i denotes the i-th stimulus, $r(i)$ is the release corresponding to the i-th stimulus, and $r(i)/r(1)$

represents the normalized amplitude of the i-th EPSC in the train. The values for fe and α were determined by solving equations (2) and (3).

Light-evoked miniature EPSCs were recorded at –70 mV and desynchronized by replacing Ca^{2+} with 4 mM Sr^{2+} and raising Mg^{2+} concentration to 4 mM (Dodge Hr. et al., 1969). To ensure that light-evoked responses are monosynaptic, recordings were performed in the presence of 1 μM TTX and 100 μM 4-AP (Petreanu et al., 2009; Whitt et al., 2022). Only cells with series resistance <25 MΩ (with <25% variation over the experiment) were included. Data was filtered at 4 kHz and digitized at 10 kHz using Igor Pro (Wave Metrics).

Biocytin processing

After recordings, slices were fixed in 4% paraformaldehyde overnight at 4°C. Slices were rinsed 2 × 10 min in 0.1 M phosphate buffer (PB) containing 19 mM $NaH_2PO_4 \cdot H2O$ and 81 mM Na_2HPO_4 at room temperature and permeabilized in 2% Triton X-100 in 0.1 mM PB for 1 h. Slices were then incubated in avidin-Alexa Fluor 633 conjugate diluted 1:2000 in 1% Triton X-100/0.1 M PB overnight at 4°C in the dark. After the incubation, slices were washed 2 × 10 min in 0.1 M PB, mounted on glass slides, and allowed to dry overnight in the dark. Slides were coverslipped with Prolong Anti-fade (Invitrogen) mounting medium and sealed with nail polish. Images were taken using a Zeiss LSM 700 confocal microscope.

Virus injection and cranial window implantation

For two-photon calcium imaging, GCaMP6s was expressed in dLGN (from Bregma AP: 2.1 mm, ML: 2.2 mm, DV: 2.5 mm) using adeno-associated virus (AAV) purchased from AAV5-Ef1a-DIO-Synaptophysin-GCaMP6s (addgene, Cat# 105715-AAV5, 2.0 x 10^{13} GS/ml) injected via a Hamilton syringe attached to a Microsyringe Pump Controller (World Precision Instruments) at a rate of 100 nl/min, total volume of 750 ul to adult (>postnatal day 90, P>90) VGluT2-Cre mice (Jax strain 028863).

A cranial window consisting of two 3 mm diameter coverslips glued with optical adhesive (Norland71, Edmund Optics) to a 5 mm diameter coverslip) was implanted. The gap between the skull and glass was sealed with silicone elastomer (Kwik-Sil). Instant adhesive Loctite 454 (Henkel) was used to adhere an aluminum head post to skull, and to cover the exposed skull, then black dental cement (iron oxide powder, AlphaChemical mixed with white powder, Dentsply) was used to coat the surface to minimize light reflections. Subjects were imaged after more than at least 3 weeks of recovery.

Two-photon imaging

Awake subjects were placed in a holding tube and immobilized by a head post clamp. Prior to the first imaging session, the subjects were habituated to the holding tube at least twice for >30 min. A shield was placed around the gap between the cranial window and the objective lens to prevent light from the visual stimuli during imaging. An Olympus FVMPE-RS Multiphoton Laser Scanning Microscope controlled by Fluoview software with a 25x NA 1.05 water immersion objective lens was used to acquire time lapse fluorescence images. An Insight X3-OL laser was tuned to 940 nm, the excitation

wavelength conventionally used for GCaMP (Ex max 490 nm). Fluorescence emission was detected through a dichroic mirror (495-540 nm). The field of view was 169.71 um x 169.71.41 um (512x512 pixels), 360±40 um from the brain surface. Minimum laser power (59 mW) and PMT gain (400) necessary to image at this depth was used. As previously reported, no photobleaching with these imaging parameters (Murase et al., 2022). Images was acquired at 28 Hz by single direction scanning. Using Suite2p package (Pachitariu et al., 2017), movement artifacts was corrected using the average intensity of the full image stack as a template. Region of interests (ROIs) was detected by axon/bouton mode (correction factor, 0.7).

For visual responses of boutons, subjects received monocular visual stimuli controlled by PsychToolBox plugin in MATLAB, (random order of 5 repeats of 12 orientations of square grating drifting at 1 Hz) at 0.05 cycle/degree (cpd), 100% contrast (28 cd/m^2) for 2.5 s interleaved with 2.5 s intensity-matched grey scale) delivered by a 23" display (Acer LCD Monitor) 28 cm in front of the eyes. To calculate $\Delta F/F = (F-F0)/F0$, where F corresponds to the fluorescence intensity at a given time point and F0 corresponds to mean fluorescent intensity during 1 s before the visual stimulus onset.

If peak $\Delta F/F$ value during 0.25 to 2.0 sec after visual stimulation onset at any direction exceeds 4 x STD of baseline (F0, -1.0 to 0 sec) for 40% or more of trials during either contra or ipsi eye stimulation, and if its mean $\Delta F/F$ of the bouton during a rising phase of response (0.25 to 1.0 sec after visual stimulus onset) as compared to the baseline exceeds 2 x signal/noise ratio (SNR), the bouton is defined as visually responsive.

Statistics

An unpaired two-tailed Student's T-test was used to determine the significance between two independent experimental groups. Mann-Whitney instead of Student's T-test was applied for EM analyses because abnormal distribution potentially caused by the presence of two distinctive classes of synapses (CC and TC). One-way ANOVA was used to determine the significance between three or more independent experimental groups. Kruskal-Wallis was used if abnormal distribution was predicted. For spike train experiments, two-way ANOVA was used.

Acknowledgement

This work was supported by R01EY016431 (EMQ) EY025922 (AK and EMQ), R01EY12124 (AK), and NICHD IRP (LD).

Figure Legends

Fig. 1. DE/LRx induces bidirectional changes in presynaptic properties of thalamo-cortical synapses in adult mouse V1b L4. a) Confirmation that C57BL/6J mice injected with AAV-CaMKIIa-hChR2-mCherry (red) effectively transfected dLGN. Thalamus displayed in bright field pictures shows overlay with confocal image of mCherry. The inset shows dLGN neurons counterstained with DAPI (blue) and expressing ChR2-mCherry. b) Example of a principal neuron in layer 4 V1b recorded and filled with biocytin (yellow). Note the substantial presence of ChR2-mCherry-positive processes, particularly in L4. No ChR2-expressing neurons were detected in V1. c) Representative examples of light-evoked EPSCs (470 nm, 3 msec) in layer 4 V1b desynchronized by Sr^{2+} and means for NR, DE, and LRx. d) Desynchronized evoked EPSCs were unchanged by DE (grey) and decreased after LRx (2 hr, yellow; mean evEPSC±sem: NR (blue), 12.9±0.7 pA; DE 13.0±0.6 pA; LRx 11.2±0.4 pA; n = 31, 26, 25 cells from 6, 5, 5 subjects, respectively, Kruskal-Wallis H (2) = 10.39, p = 0.0055, post hoc Dunn's multiple comparison test. e) Repetitive optogenetic stimulation in the absence of Sr^{2+} (15 pulses of 470 nm LED for 3 msec at 25 Hz at intensity that evoked 100% response). f) Normalized EPSC trains. Visual experience modifies EPSC amplitudes (n = 32, 23, 21 cells from 8, 6, 5 subjects for NR, DE, LRx, respectively. Repeated measures ANOVA, F = 63.3, p < 0.0001, post hoc Bonferroni). g) Normalized EPSC at steady state. h) Paired pulse ratio (EPSCs for spike#2/spike#1) is increased by DE and decreased by LRx. i) Presynaptic release probability is decreased by DE and increased by LRx. j) LRx decreases synaptic vesicle recovery rate.

Fig. 2. DE/LRx modify ultrastructure of excitatory synapses in layer 4 of adult mouse V1b. a) Overlays depict sampling area in layer 4 and the structure quantified for presynaptic area, cleft width, PSD length, docked vesicles and synaptic vesicle zone area. The distribution of synaptic profiles by presynaptic area reveals two peaks: the larger population (>0.6 μm^2; purple) has significantly larger cleft widths, PSD lengths, docked vesicles and synaptic vesicle areas. b) Experimental timeline. Adult C57B/L6 mice (>P90) received 10 days of DE (left) followed by 2 h of LRx (right). Expression of each ultrastructural parameter (Y axis) relative to presynaptic area (X axis). Distribution of each parameter is shown separately at top and right. DE (grey) significantly decreases synaptic cleft width and PSD length, and increases the number of docked vesicles, SVZ area. LRx (yellow) significantly decreases SVZ area, *p<0.001 Mann-Whitney Test. 264, 219, 320 synapses from 5, 4, 6 subjects for control (Con; blue), DE and LRx.

Fig. 3. DE/LRx induce reversible changes in Bsn clustering in thalamic boutons of adult mouse V1b L4. a) Experimental logic of FRET-based proximity assay. b) Serial dilution of secondary antibodies carrying donor and acceptor fluorophores decreases $FRET_{A/D}$ ratio. Box plots represent the median as a bar, 25th to 75th percentile as box, and max and min as whiskers (n = 2343, 2304, 970 puncta from 3 subjects each condition; One-way ANOVA, F = 1731, p<0.0001, *post hoc* Tukey, *p<0.01). c) Examples of Bsn immunofluorescence of donor (orange, AF568) and acceptor (red, AF647) immunofluorescence from layer 4 of adult mouse V1b of Con, DE (10 d), and LRx (2 hr) subjects. d) $R_{A/D}$ values at VGluT2 puncta average by subject for Con, DE,

LRx subjects (n = 4, 4, 4; One-way ANOVA, F = 13.0, *p = 0.002, post hoc Tukey, *p<0.01). Right: $R_{A/D}$ of 100 puncta from each subject. e) Bsn immunofluorescence visualized with single secondary antibody is similar across groups (One-way ANOVA, F = 1.0, p = 0.41. Right: Bsn immunofluorescence of 100 puncta from each subject).

Fig. 4. DE/LRx induce reversible changes in the magnitude of visually evoked calcium transients in dLGN boutons recorded in layer 4 of adult mouse V1b. a) AAV-Ef1a-DIO-synaptophysin-GCaMP6s (900 µl) was delivered at 0.1 µl/min to dLGN: AP: 2.1 mm, ML: 2.2 mm, DV: 2.5 mm from bregma. 2P live imaging of axonal GCaMP in head-fixed awake adult mice. Cartoon depicting the abundance of thalamic axons throughout V1b. b) 2P live imaging of axonal GCaMP6. Heat map depicting magnitude of visually-evoked $\Delta F/F$ for control (Con), DE and LRx subjects (gray—<0.3, blue—0.3 to 0.6, purple—0.6 to 0.9, orange—0.9 to 1.2, pink—>1.2). c) Representative examples of visually evoked GCaMP transients in single axonal boutons in response to 100% contrast, 0.05 cpd, square wave gratings of 12 directions drifting at 1 Hz. d) Left: Visually-evoked GCaMP $\Delta F/F$ in thalamic boutons, evoked by stimulus of preferred orientation, and recorded in layer 4 of adult mouse V1b, averaged by subject (258, 2451, 1572 boutons from n = 4, 4, 4 subjects for Con, DE, LRx. One-way ANOVA, F = 9.9, p=0.005, post hoc Tukey, *p<0.01).). Right: $\Delta F/F$ for 30 boutons per subject.

References

Andrade-Talavera Y, Pérez-Rodríguez M, Prius-Mengual J, Rodríguez-Moreno A (2023) Neuronal and astrocyte determinants of critical periods of plasticity. Trends Neurosci 46:566–580 Available at: https://doi.org/10.1016/j.tins.2023.04.005.

Antonini A, Stryker MP (1993) Rapid Remodeling of Axonal Arbors in the Visual Cortex. Science (80-) 260:1819–1821.

Antonini A, Stryker MP (1996) Plasticity of geniculocortical afferents following brief or prolonged monocular occlusion in the cat. J Comp Neurol 369:64–82.

Bacci A, Coco S, Pravettoni E, Schenk U, Armano S, Frassoni C, Verderio C, De Camilli P, Matteoli M (2001) Chronic blockade of glutamate receptors enhances presynaptic release and downregulates the interaction between synaptophysin-synaptobrevin-vesicle-associated membrane protein 2. J Neurosci 21:6588–6596.

Balcioglu A, Gillani R, Doron M, Burnell K, Ku T, Erisir A, Chung K, Segev I, Nedivi E (2023) Mapping thalamic innervation to individual L2/3 pyramidal neurons and modeling their ‘readout’ of visual input. Nat Neurosci 26:470–480.

Blundon JA, Roy NC, Teubner BJW, Yu J, Eom T-Y, Sample KJ, Pani A, Smeyne RJ, Han SB, Kerekes RA, Rose DC, Hackett TA, Vuppala PK, Freeman BB, Zakharenko SS (2017) Restoring auditory cortex plasticity in adult mice by restricting thalamic adenosine signaling. Science 356:1352–1356 Available at: http://www.ncbi.nlm.nih.gov/pubmed/28663494.

Bopp R, Holler-Rickauer S, Martin KAC, Schuhknecht GFP (2017) An ultrastructural study of the thalamic input to layer 4 of primary motor and primary somatosensory cortex in the mouse. J Neurosci 37:2435–2448.

Borczyk M, Śliwińska MA, Caly A, Bernas T, Radwanska K (2019) Neuronal plasticity affects correlation between the size of dendritic spine and its postsynaptic density. Sci Rep 9:1–12.

Borges-Merjane C, Kim O, Jonas P (2020) Functional Electron Microscopy, “Flash and Freeze,” of Identified Cortical Synapses in Acute Brain Slices. Neuron 105:992-1006.e6 Available at: https://doi.org/10.1016/j.neuron.2019.12.022.

Bridi MCD, de Pasquale R, Lantz CL, Gu Y, Borrell A, Choi S-Y, He K, Tran T, Hong SZ, Dykman A, Lee H-K, Quinlan EM, Kirkwood A (2018) Two distinct mechanisms for experience-dependent homeostasis. Nat Neurosci 21:843–850 Available at: http://www.nature.com/articles/s41593-018-0150-0 [Accessed February 28, 2019].

Bridi MS, Shin S, Huang S, Kirkwood A (2020) Dynamic Recovery from Depression Enables Rate Encoding in Inhibitory Synapses. iScience 23:100940 Available at: https://doi.org/10.1016/j.isci.2020.100940.

Burrone J, O’Byrne M, Murthy VN (2002) Multiple forms of synaptic plasticity triggered by selective suppression of activity in individual neurons. Nature 420:414–418.

Cheng MY, Wang EH, Woodson WJ, Wang S, Sun G, Lee AG, Arac A, Fenno LE, Deisseroth K, Steinberg GK (2014) Optogenetic neuronal stimulation promotes functional recovery after stroke. Proc Natl Acad Sci U S A 111:12913–12918.

Chokshi V, Gao M, Grier BD, Owens A, Wang H, Worley PF, Lee HK (2019) Input-Specific Metaplasticity in the Visual Cortex Requires Homer1a-Mediated mGluR5 Signaling. Neuron 104:736-748.e6.

Chung S, Jeong JH, Ko S, Yu X, Kim YH, Isaac JTR, Koretsky AP (2017) Peripheral Sensory Deprivation Restores Critical-Period-like Plasticity to Adult Somatosensory

Thalamocortical Inputs. Cell Rep 19:2707–2717 Available at: http://dx.doi.org/10.1016/j.celrep.2017.06.018.

Chung S, Li X, Nelson SB (2002) Short-term depression at thalamocortical synapses contributes to rapid adaptation of cortical sensory responses in vivo. Neuron 34:437–446.

Cole AA, Reese TS (2023) Transsynaptic Assemblies Link Domains of Presynaptic and Postsynaptic Intracellular Structures across the Synaptic Cleft. J Neurosci 43:5883–5892.

Coleman JE, Nahmani M, Gavornik JP, Haslinger R, Heynen AJ, Erisir A, Bear MF (2010) Rapid Structural Remodeling of Thalamocortical Synapses Parallels Experience-Dependent Functional Plasticity in Mouse Primary Visual Cortex. J Neurosci 30:9670–9682 Available at: www.jneurosci.org.

Cooper LN, Bear MF (2012) The BCM theory of synapse modification at 30: interaction of theory with experiment. Nat Rev Neurosci 13:798–810 Available at: http://www.nature.com/articles/nrn3353 [Accessed April 3, 2019].

Crair MC, Malenka RC (1995) A critical period for long-term potentiation at thalamocortical synapses. Nature 375:325–328 Available at: http://www.nature.com/articles/375325a0 [Accessed April 24, 2019].

Crozier RA, Wang Y, Liu CH, Bear MF (2007) Deprivation-induced synaptic depression by distinct mechanisms in different layers of mouse visual cortex. Proc Natl Acad Sci U S A 104:1383–1388.

Davis GW, Müller M (2015) Homeostatic control of presynaptic neurotransmitter release. Annu Rev Physiol 77:251–270.

Davydova D, Marini C, King C, Klueva J, Bischof F, Romorini S, Montenegro-Venegas C, Heine M, Schneider R, Schröder MS, Altrock WD, Henneberger C, Rusakov DA, Gundelfinger ED, Fejtova A (2014) Bassoon specifically controls presynaptic P/Q-type Ca2+ channels via RIM-binding protein. Neuron 82:181–194.

Delvendahl I, Müller M (2019) Homeostatic plasticity—a presynaptic perspective. Curr Opin Neurobiol 54:155–162.

Dodge Jr. FA, Miledi R, Rahamimoff R (1969) Strontium and quantal release of transmitter at the neuromuscular junction. J Physiol 200:267–283 Available at: https://doi.org/10.1113/jphysiol.1969.sp008692.

Duffy KR, Lingley AJ, Holman KD, Mitchell DE (2016) Susceptibility to monocular deprivation following immersion in darkness either late into or beyond the critical period. J Comp Neurol 524:2643–2653.

Eaton NC, Sheehan HM, Quinlan EM (2016) Optimization of visual training for full recovery from severe amblyopia in adults. Learn Mem 23:99–103.

Echegoyen J, Neu A, Graber KD, Soltesz I (2007) Homeostatic plasticity studies using in vivo hippocampal activity-blockade: Synaptic scaling, intrinsic plasticity and age-dependence. PLoS One 2.

Favre D, Scarfone E, Di Gioia G, De Camilli P, Dememes D (1986) Presence of synapsin I in afferent and efferent nerve endings of vestibular sensory epithelia. Brain Res 384:379–382 Available at: http://www.embase.com/search/results?subaction=viewrecord&from=export&id=L17660784%0Ahttp://sfx.library.uu.nl/utrecht?sid=EMBASE&issn=00068993&id=doi:&atitle=Presence+of+synapsin+I+in+afferent+and+efferent+nerve+endings+of+vesti

bular+sensory+epithelia.&st.

Feldman DE, Nicoll RA, Malenka RC, Isaac JTR (1998) Long-term depression at thalamocortical synapses in developing rat somatosensory cortex. Neuron 21:347–357.

Finger TE, Womble M, Kinnamon JC, Ueda T (1990) Synapsin I-like immunoreactivity in nerve fibers associated with lingual taste buds of the rat. J Comp Neurol 292:283–290.

Frantz MG, Crouse EC, Sokhadze G, Ikrar T, Stephany C-É, Nguyen C, Xu X, McGee AW (2020) Layer 4 Gates Plasticity in Visual Cortex Independent of a Canonical Microcircuit. Curr Biol 30:1–12.

Gao M, Sossa K, Song L, Errington L, Cummings L, Hwang H, Kuhl D, Worley P, Lee HK (2010) A specific requirement of Arc/Arg3.1 for visual experience-induced homeostatic synaptic plasticity in mouse primary visual cortex. J Neurosci 30:7168–7178.

Glebov OO, Cox S, Humphreys L, Burrone J (2016) Neuronal activity controls transsynaptic geometry. Sci Rep 6:1–11 Available at: http://dx.doi.org/10.1038/srep22703.

Glebov OO, Jackson RE, Winterflood CM, Owen DM, Barker EA, Doherty P, Ewers H, Burrone J (2017) Nanoscale Structural Plasticity of the Active Zone Matrix Modulates Presynaptic Function. Cell Rep 18:2715–2728 Available at: http://dx.doi.org/10.1016/j.celrep.2017.02.064.

Goel A, Jiang B, Xu LW, Song L, Kirkwood A, Lee H-K (2006) Cross-modal regulation of synaptic AMPA receptors in primary sensory cortices by visual experience. Nat

Neurosci 9:1001–1003 Available at: http://www.nature.com/articles/nn1725 [Accessed March 1, 2019].

Goel A, Lee H-K (2007) Persistence of Experience-Induced Homeostatic Synaptic Plasticity through Adulthood in Superficial Layers of Mouse Visual Cortex. J Neurosci 27:6692–6700 Available at: http://www.jneurosci.org/cgi/doi/10.1523/JNEUROSCI.5038-06.2007.

Gundelfinger ED, Reissner C, Garner CC (2016) Role of Bassoon and Piccolo in Assembly and Molecular Organization of the Active Zone. Front Synaptic Neurosci 7.

Haas CA, DeGennaro LJ, Muller M, Hollander H (1990) Synapsin I expression in the rat retina during postnatal develpment. Exp Brain Res 82:25–32.

Harris KP, Littleton JT (2015) Transmission, development, and plasticity of synapses. Genetics 201:345–375.

He H-Y, Ray B, Dennis K, Quinlan EM (2007) Experience-dependent recovery of vision following chronic deprivation amblyopia. Nat Neurosci 10:1134–1136 Available at: papers3://publication/doi/10.1038/nn1965.

He HY, Hodos W, Quinlan EM (2006) Visual deprivation reactivates rapid ocular dominance plasticity in adult visual cortex. J Neurosci 26:2951–2955.

Hosokawa T, Liu PW, Cai Q, Ferreira JS, Levet F, Butler C, Sibarita JB, Choquet D, Groc L, Hosy E, Zhang M, Hayashi Y (2021) CaMKII activation persistently segregates postsynaptic proteins via liquid phase separation. Nat Neurosci 24:777–785 Available at: http://dx.doi.org/10.1038/s41593-021-00843-3.

Huh CYL, Abdelaal K, Salinas KJ, Gu D, Zeitoun J, Figueroa Velez DX, Peach JP,

Fowlkes CC, Gandhi SP (2020) Long-term Monocular Deprivation during Juvenile Critical Period Disrupts Binocular Integration in Mouse Visual Thalamus. J Neurosci 40:585–604 Available at: https://www.jneurosci.org/content/40/3/585 [Accessed June 26, 2020].

Isaac JTR, Crair MC, Nicoll RA, Malenka RC (1997) Silent synapses during development of thalamocortical inputs. Neuron 18:269–280.

Jaepel J, Hübener M, Bonhoeffer T, Rose T (2017) Lateral geniculate neurons projecting to primary visual cortex show ocular dominance plasticity in adult mice. Nat Neurosci 20:1708–1714 Available at: http://www.nature.com/articles/s41593-017-0021-0 [Accessed January 15, 2019].

Jeon BB, Fuchs T, Chase SM, Kuhlman SJ (2022) Visual experience has opposing influences on the quality of stimulus representation in adult primary visual cortex. Elife 11:1–18.

Jiang B, Trevino M, Kirkwood A (2007) Sequential Development of Long-Term Potentiation and Depression in Different Layers of the Mouse Visual Cortex. J Neurosci 27:9648–9652 Available at: http://www.jneurosci.org/cgi/doi/10.1523/JNEUROSCI.2655-07.2007.

Kaeser PS, Regehr WG (2017) The readily releasable pool of synaptic vesicles. Curr Opin Neurobiol 43:63–70 Available at: http://dx.doi.org/10.1016/j.conb.2016.12.012.

Kloc M, Maffei A (2014) Target-specific properties of thalamocortical synapses onto layer 4 of mouse primary visual cortex. J Neurosci 34:15455–15465.

Lee HK, Kirkwood A (2019) Mechanisms of Homeostatic Synaptic Plasticity in vivo. Front Cell Neurosci 13:1–7.

Linden ML, Heynen AJ, Haslinger RH, Bear MF (2009) Thalamic activity that drives visual cortical plasticity. Nat Neurosci 12:390–392 Available at: http://www.nature.com/articles/nn.2284 [Accessed January 4, 2019].

Lu HC, Mackie K (2021) Review of the Endocannabinoid System. Biol Psychiatry Cogn Neurosci Neuroimaging 6:607–615 Available at: https://doi.org/10.1016/j.bpsc.2020.07.016.

Mainardi M, Landi S, Gianfranceschi L, Baldini S, De Pasquale R, Berardi N, Maffei L, Caleo M (2010) Environmental enrichment potentiates thalamocortical transmission and plasticity in the adult rat visual cortex. J Neurosci Res 88:3048–3059.

Mandell JW, Czernik AJ, De Camilli P, Greengard P, Townes-Anderson E (1992) Differential expression of synapsins I and II among rat retinal synapses. J Neurosci 12:1736–1749.

Masch JM, Steffens H, Fischer J, Engelhardt J, Hubrich J, Keller-Findeisen J, D'Este E, Urban NT, Grant SGN, Sahl SJ, Kamin D, Hell SW (2018) Robust nanoscopy of a synaptic protein in living mice by organic-fluorophore labeling. Proc Natl Acad Sci U S A 115:E8047–E8056.

Meyer D, Bonhoeffer T, Scheuss V (2014) Balance and stability of synaptic structures during synaptic plasticity. Neuron 82:430–443 Available at: http://dx.doi.org/10.1016/j.neuron.2014.02.031.

Min SH, Wang Z, Chen MT, Hu R, Gong L, He Z, Wang X, Hess RF, Zhou J (2023) Metaplasticity: Dark exposure boosts local excitability and visual plasticity in adult human cortex. J Physiol 601:4105–4120.

Mitra A, Mitra SS, Tsien RW (2012) Heterogeneous reallocation of presynaptic efficacy

in recurrent excitatory circuits adapting to inactivity. Nat Neurosci 15:250–257.

Montenegro-Venegas C, Guhathakurta D, Pina-Fernandez E, Andres-Alonso M, Plattner F, Gundelfinger ED, Fejtova A (2022) Bassoon controls synaptic vesicle release via regulation of presynaptic phosphorylation and cAMP . EMBO Rep 23:1–20.

Montey KL, Quinlan EM (2011) Recovery from chronic monocular deprivation following reactivation of thalamocortical plasticity by dark exposure. Nat Commun 2.

Murase S, Lantz CL, Quinlan EM (2017) Light reintroduction after dark exposure reactivates plasticity in adults via perisynaptic activation of MMP-9. Elife 6.

Murase S, Robertson SE, Lantz CL, Liu J, Winkowski DE, Quinlan EM (2022) Chronic Monocular Deprivation Reveals MMP9-Dependent and -Independent Aspects of Murine Visual System Plasticity. Int J Mol Sci 23:2438.

Murase S, Winkowski DE, Liu J, Kanold PO, Elizabeth M. Quinlan (2019) Homeostatic regulation of perisynaptic MMP9 activity in the amblyopic visual cortex. Elife 8:1–18.

Murthy VN et al. (2001) Inactivity Produces Increases in Neurotransmitter Release and Synapse Size. Neuron 32:673–682 Available at: http://www.cell.com/neuron/fulltext/S0896-6273(01)00500-1%5Cnhttp://linkinghub.elsevier.com/retrieve/pii/S0896627301005001.

Nahmani M, Erisir A (2005) VGluT2 immunochemistry identifies thalamocortical terminals in layer 4 of adult and developing visual cortex. J Comp Neurol 484:458–473 Available at: http://doi.wiley.com/10.1002/cne.20505 [Accessed May 8, 2020].

Nair D, Hosy E, Petersen JD, Constals A, Giannone G, Choquet D, Sibarita JB (2013)

Super-resolution imaging reveals that AMPA receptors inside synapses are dynamically organized in nanodomains regulated by PSD95. J Neurosci 33:13204–13224.

Oberlaender M, Ramirez A, Bruno RM (2012) Sensory Experience Restructures Thalamocortical Axons during Adulthood. Neuron 74:648–655 Available at: http://dx.doi.org/10.1016/j.neuron.2012.03.022.

Owe SG, Erisir A, Heggelund P (2013) Terminals of the major thalamic input to visual cortex are devoid of synapsin proteins. Neuroscience 243:115–125 Available at: http://dx.doi.org/10.1016/j.neuroscience.2013.03.031.

Pachitariu M, Stringer C, Dipoppa M, Schröder S, Rossi LF, Dalgleish H, Carandini M, Harris KD (2017) Suite2p: beyond 10,000 neurons with standard two-photon microscopy. bioRxiv. Bioarxiv 20:2017.

Petreanu L, Mao T, Sternson SM, Svoboda K (2009) The subcellular organization of neocortical excitatory connections. Nature 457:1142–1145.

Petrus E, Isaiah A, Jones AP, Li D, Wang H, Lee HK, Kanold PO (2014) Crossmodal Induction of Thalamocortical Potentiation Leads to Enhanced Information Processing in the Auditory Cortex. Neuron 81:664–673 Available at: http://dx.doi.org/10.1016/j.neuron.2013.11.023.

Petrus E, Rodriguez G, Patterson R, Connor B, Kanold PO, Lee H-K (2015) Vision loss shifts the balance of feedforward and intracortical circuits in opposite directions in mouse primary auditory and visual cortices. J Neurosci 35:8790–8801 Available at: http://www.jneurosci.org/content/35/23/8790.abstract?etoc.

Qin Y, Ahmadlou M, Suhai S, Neering P, de Kraker L, Heimel JA, Levelt CN (2023)

Thalamic regulation of ocular dominance plasticity in adult visual cortex. Elife 12:1–17.

Sale A, Maya Vetencourt JF, Medini P, Cenni MC, Baroncelli L, De Pasquale R, Maffei L (2007) Environmental enrichment in adulthood promotes amblyopia recovery through a reduction of intracortical inhibition. Nat Neurosci 10:679–681.

Savtchenko LP, Rusakov DA (2007) The optimal height of the synaptic cleft. Proc Natl Acad Sci U S A 104:1823–1828.

Schoonover CE, Tapia JC, Schilling VC, Wimmer V, Blazeski R, Zhang W, Mason CA, Bruno RM (2014) Comparative strength and dendritic organization of thalamocortical and corticocortical synapses onto excitatory layer 4 neurons. J Neurosci 34:6746–6758.

Stodieck SK, Greifzu F, Goetze B, Schmidt KF, Löwel S (2014) Brief dark exposure restored ocular dominance plasticity in aging mice and after a cortical stroke. Exp Gerontol 60:1–11 Available at: http://dx.doi.org/10.1016/j.exger.2014.09.007.

Stratford KJ, Tarczy-Hornoch K, Martin KAC, Bannister NJ, Jack JJB (1996) Excitatory synaptic inputs to spiny stellate cells in cat visual cortex. Nature 382:258–261.

Sun W, Tan Z, Mensh BD, Ji N (2016) Thalamus provides layer 4 of primary visual cortex with orientation- and direction-tuned inputs. Nat Neurosci 19:308–315.

Tennant KA, Taylor SL, White ER, Brown CE (2017) Optogenetic rewiring of thalamocortical circuits to restore function in the stroke injured brain. Nat Commun 8:1–14 Available at: http://dx.doi.org/10.1038/ncomms15879.

Tokuoka H, Goda Y (2008) Activity-dependent coordination of presynaptic release probability and postsynaptic GluR2 abundance at single synapses. Proc Natl Acad

Sci U S A 105:14656–14661.

Valakh V, Wise D, Zhu XA, Sha M, Fok J, Van Hooser SD, Schectman R, Cepeda I, Kirk R, O'toole S, Nelson SB (2023) A transcriptional constraint mechanism limits the homeostatic response to activity deprivation in mammalian neocortex Abbreviated Title: HLF and TEF regulate homeostatic plasticity. Elife 12:1–25.

Wang L, Kloc M, Gu Y, Ge S, Maffei A (2013) Layer-specific experience-dependent rewiring of thalamocortical circuits. J Neurosci 33:4181–4191.

Wen W, Turrigiano GG (2024) Keeping Your Brain in Balance: Homeostatic Regulation of Network Function. Annu Rev Neurosci 47:41–61.

Wesseling JF, Lo DC (2002) Limit on the role of activity in controlling the release-ready supply of synaptic vesicles. J Neurosci 22:9708–9720.

Whitt JL, Ewall G, Chakraborty D, Adegbesan A, Lee R, Kanold PO, Lee HK (2022) Visual Deprivation Selectively Reduces Thalamic Reticular Nucleus-Mediated Inhibition of the Auditory Thalamus in Adults. J Neurosci 42:7921–7930.

Wiesel TN, Hubel DH (1963) Responses in Striate Deprived of Vision Cortex of One Eye. J Neurophysiol 26:1003–1017.

Wise DL, Greene SB, Escobedo-Lozoya Y, Van Hooser SD, Nelson SB (2024) Progressive Circuit Hyperexcitability in Mouse Neocortical Slice Cultures with Increasing Duration of Activity Silencing. eNeuro 11:1–14.

Yanagisawa T, Tsumoto T, Kimura F (2004) Transiently higher release probability during critical period at thalamocortical synapses in the mouse barrel cortex: Relevance to differential short-term plasticity of AMPA and NMDA EPSCs and possible involvement of silent synapses. Eur J Neurosci 20:3006–3018.

Yu Q, Zhang P, Qiu J, Fang F (2016) Perceptual Learning of Contrast Detection in the Human Lateral Geniculate Nucleus. Curr Biol 26:3176–3182 Available at: http://dx.doi.org/10.1016/j.cub.2016.09.034.

Yu X, Chung S, Chen DY, Wang S, Dodd SJ, Walters JR, Isaac JTR, Koretsky AP (2012) Thalamocortical Inputs Show Post-Critical-Period Plasticity. Neuron 74:731–742 Available at: http://dx.doi.org/10.1016/j.neuron.2012.04.024.

Zheng K, Jensen TP, Savtchenko LP, Levitt JA, Suhling K, Rusakov DA (2017) Nanoscale diffusion in the synaptic cleft and beyond measured with time-resolved fluorescence anisotropy imaging. Sci Rep 7:1–10.

Ziv G, Connors BW, Amitai Y (1999) Efficacy of thalamocortical and intracortical synaptic connections: Quanta, innervation, and reliability. Neuron 23:385–397.

Zuber B, Nikonenko I, Klauser P, Muller D, Dubochet J (2005) The mammalian central nervous synaptic cleft contains a high density of periodically organized complexes. Proc Natl Acad Sci U S A 102:19192–19197.

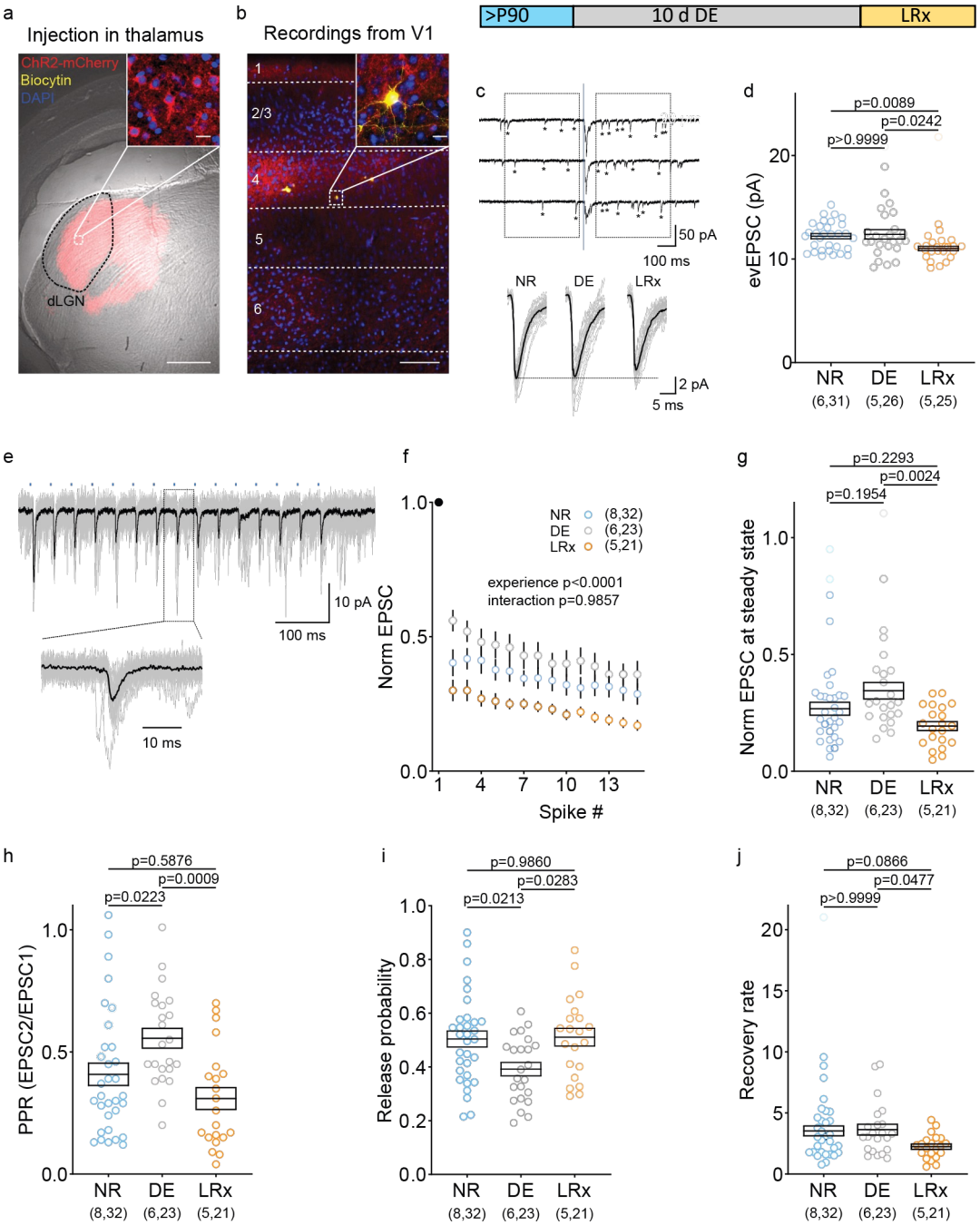
a
Injection in thalamus
ChR2-mCherry
Biocytin
DAPI
dLGN
b
Recordings from V1
1
2/3
4
5
6
>P90
10 d DE
LRx
c
50 pA
100 ms
NR
DE
LRx
2 pA
5 ms
d
p=0.0089
p=0.0242
p>0.9999
eEPSC (pA)
NR
DE
LRx
(6,31)
(5,26)
(5,25)
e
10 pA
100 ms
10 ms
f
NR (8,32)
DE (6,23)
LRx (5,21)
experience p<0.0001
interaction p=0.9857
Norm EPSC
Spike #
g
p=0.2293
p=0.0024
p=0.1954
Norm EPSC at steady state
NR
DE
LRx
(8,32)
(6,23)
(5,21)
h
p=0.5876
p=0.0009
p=0.0223
PPR (EPSC2/EPSC1)
NR
DE
LRx
(8,32)
(6,23)
(5,21)
i
p=0.9860
p=0.0283
p=0.0213
Release probability
NR
DE
LRx
(8,32)
(6,23)
(5,21)
j
p=0.0866
p=0.0477
p>0.9999
Recovery rate
NR
DE
LRx
(8,32)
(6,23)
(5,21)

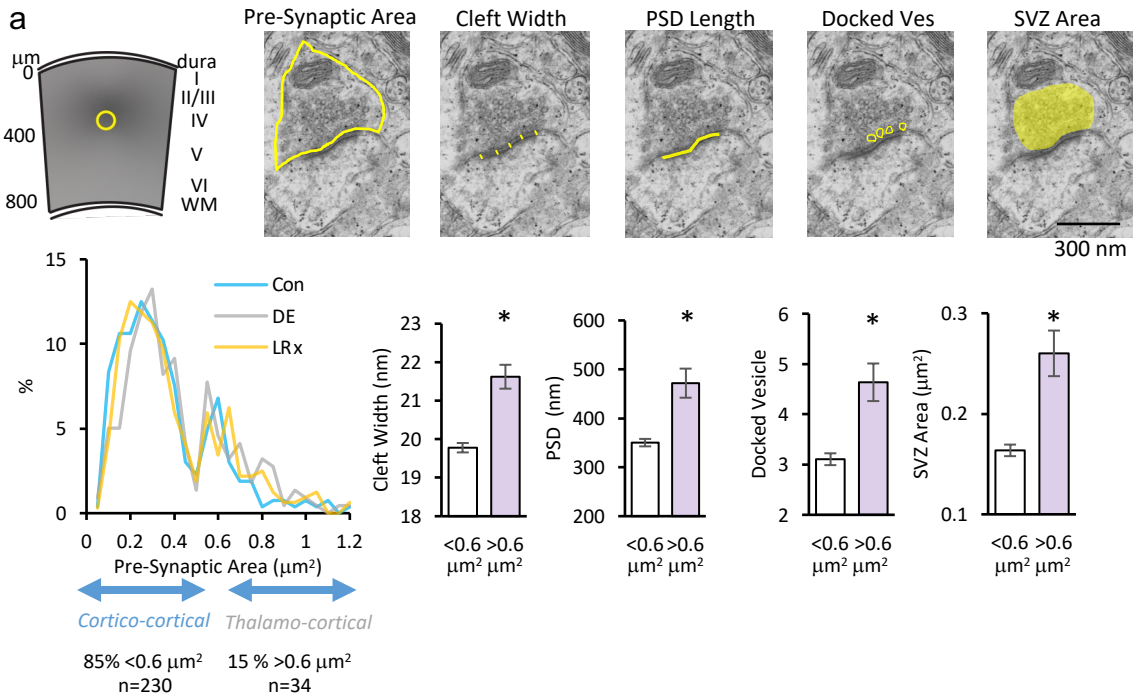
a
Pre-Synaptic Area
Cleft Width
PSD Length
Docked Ves
SVZ Area
µm
0
400
800
dura
I
II/III
IV
V
VI
WM
300 nm
Con
DE
LRx
%
Pre-Synaptic Area (µm²)
Cleft Width (nm)
PSD (nm)
Docked Vesicle
SVZ Area (µm²)
<0.6 µm²
>0.6 µm²
Cortico-cortical
Thalamo-cortical
85% <0.6 µm²
n=230
15 % >0.6 µm²
n=34

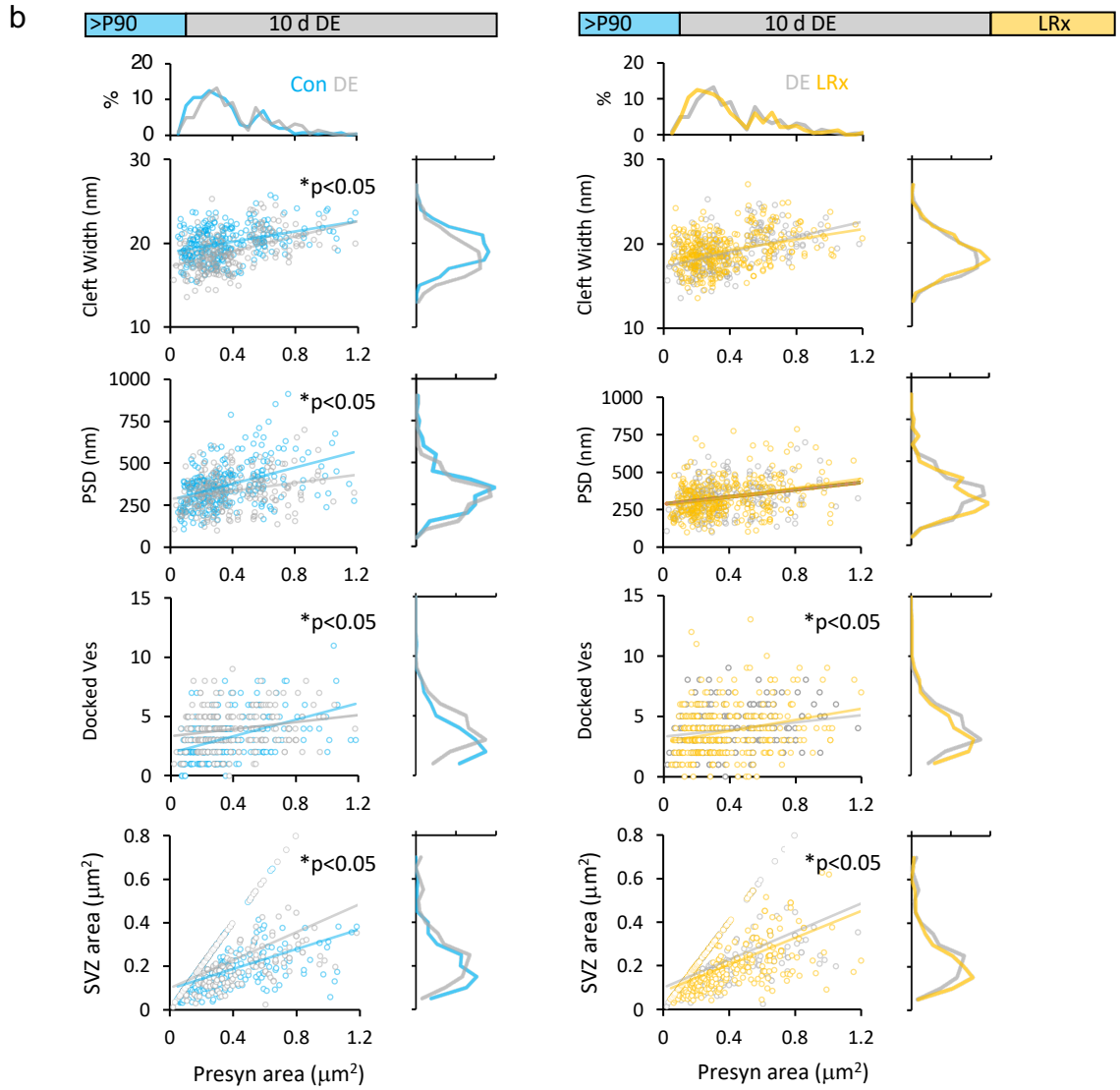
b
>P90
10 d DE
LRx
Con DE
DE LRx
%
Cleft Width (nm)
PSD (nm)
Docked Ves
SVZ area (µm²)
*p<0.05
Presyn area (µm²)

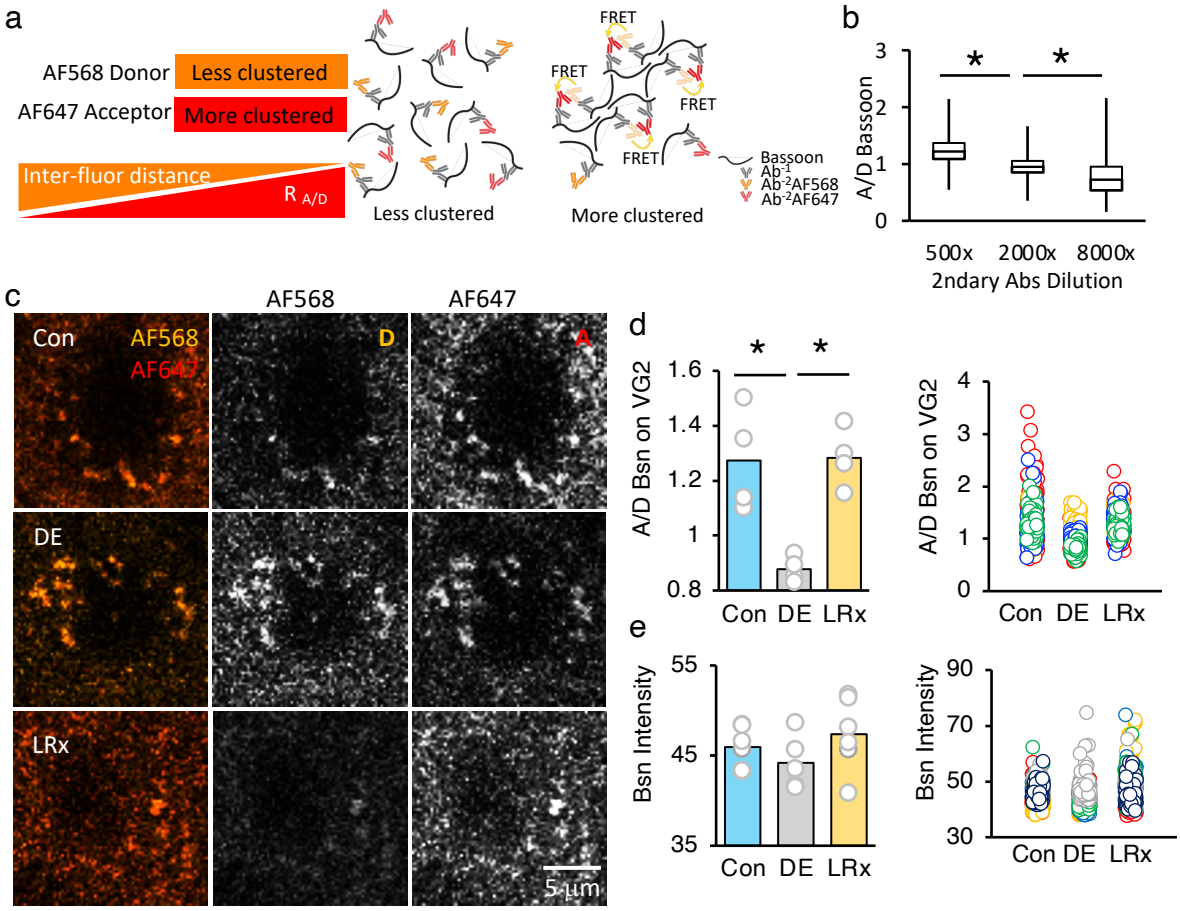
a
AF568 Donor
Less clustered
AF647 Acceptor
More clustered
Inter-fluor distance
R A/D
Less clustered
FRET
More clustered
Bassoon
Ab-1
Ab-2AF568
Ab-2AF647
b
A/D Bassoon
500x
2000x
8000x
2ndary Abs Dilution
c
AF568
AF647
Con
DE
LRx
D
A
5 µm
d
A/D Bsn on VG2
Con DE LRx
e
Bsn Intensity
Con DE LRx

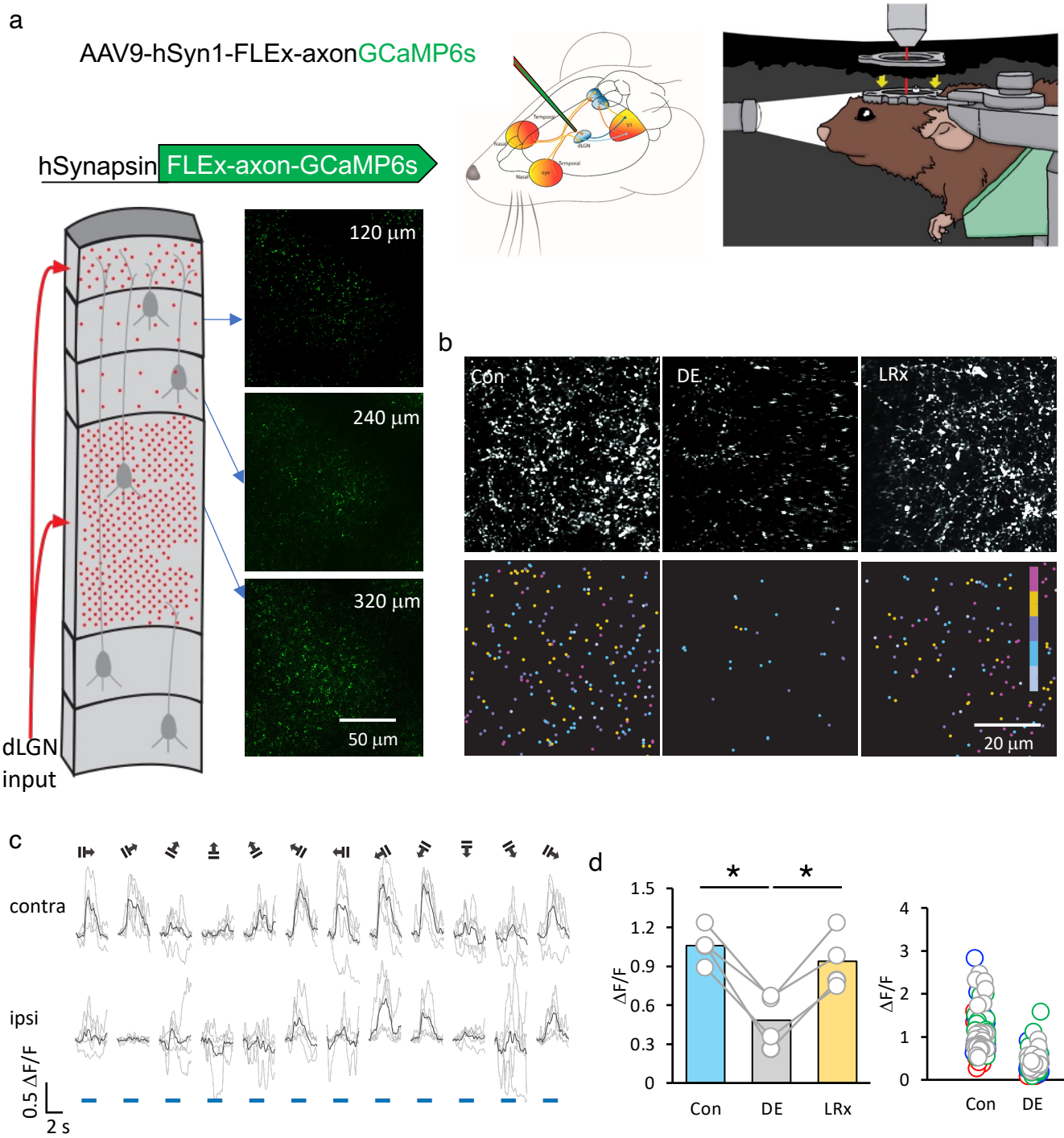
a
AAV9-hSyn1-FLEx-axonGCaMP6s
hSynapsin
FLEx-axon-GCaMP6s
120 µm
240 µm
320 µm
50 µm
dLGN
input
b
Con
DE
LRx
20 µm
c
contra
ipsi
0.5 ΔF/F
2 s
d
ΔF/F
Con
DE
LRx